Astronomy & Astrophysics

Power distribution of oscillations in the atmosphere of a plage region

Joint observations with ALMA, IRIS, and SDO

Nancy Narang[1,2] , Kalugodu Chandrashekhar[1,2] , Shahin Jafarzadeh[1,2] , Bernhard Fleck[3] ,
Mikołaj Szydlarski[1,2] , and Sven Wedemeyer[1,2]

[1] Rosseland Centre for Solar Physics, University of Oslo, PO Box 1029, Blindern 0315 Oslo, Norway
  e-mail: nancy.narang@astro.uio.no
[2] Institute of Theoretical Astrophysics, University of Oslo, PO Box 1029, Blindern 0315 Oslo, Norway
[3] ESA Science and Operations Department, c/o NASA Goddard Space Flight Center, Greenbelt, MD 20771, USA

ABSTRACT

Context. Joint observations of the Atacama Large Millimeter/Submillimeter Array (ALMA) with other solar observatories can provide a wealth of opportunities for understanding the coupling between different layers of the solar atmosphere.
Aims. We present a statistical analysis of the power distribution of oscillations in a plage region in active region NOAA AR12651, which was observed jointly with ALMA, the Interface Region Imaging Spectrograph (IRIS), and the Solar Dynamics Observatory (SDO).
Methods. We employ coordinated ALMA Band 6 (1.25 mm) brightness temperature maps, IRIS slit-jaw images in the 2796 Å passband, and observations in six passbands (1600 Å, 304 Å, 131 Å, 171 Å, 193 Å, and 211 Å) from the Atmospheric Imaging Assembly (AIA) on board SDO. We perform Lomb-Scargle transforms to study the distribution of oscillation power by means of dominant period maps and power maps. We study the spatial association of oscillations through the atmosphere, with a focus on the correlation of the power distribution of ALMA oscillations with others.
Results. We do not observe any significant association of ALMA oscillations with IRIS and AIA oscillations. While the global behavior of the dominant ALMA oscillations shows a similarity with that of the transition region and coronal passbands of AIA, the ALMA dominant period maps and power maps do not show any correlation with those from the other passbands. The spatial distribution of dominant periods and power in different period intervals of ALMA oscillations is uncorrelated with those of any other passbands.
Conclusions. We speculate that the non-association of ALMA oscillations with those of IRIS and AIA is due to significant variations in the height of formation of the millimeter continuum observed by ALMA. Additionally, the fact that ALMA directly maps the brightness temperature, in contrast to the intensity observations by IRIS and AIA, can result in the very different intrinsic nature of the ALMA oscillations compared to the IRIS and AIA oscillations.

Key words. Sun: atmosphere – Sun: faculae, plages – Sun: oscillations – Sun: radio radiation – Sun: UV radiation

1. Introduction

The solar chromosphere is a vast reservoir of magnetohydrodynamic wave energy, with numerous complex structures showing a variety of oscillatory phenomena over a wide range of magnetic environments (Narain & Ulmschneider 1990, 1996; Morton et al. 2012; Jess et al. 2015). The convective flows below the solar surface and the dynamics of the solar photosphere and chromosphere excite and manifest themselves in the form of various magnetoacoustic oscillations in these layers (e.g., Brynildsen et al. 2003; Morton et al. 2013; Jafarzadeh et al. 2013; Gafeira et al. 2017; Stangalini et al. 2017). These ubiquitous oscillations are coupled in several ways within the solar atmospheric layers and are one of the candidates for chromospheric and coronal heating (Nakariakov & Verwichte 2005; Taroyan & Erdélyi 2009; Wedemeyer-Böhm et al. 2009; Arregui 2015; Gilchrist-Millar et al. 2021).

The chromosphere, being the bridge between the relatively cool photosphere and the intensely hot corona, is the key region for understanding the heating mechanisms involved (Carlsson et al. 2019). The chromosphere is brightest in plage regions, which are mostly the chromospheric imprints of the foot-point regions of coronal loops and thus serve as efficient conduits in the mass and energy cycle of the atmosphere (Carlsson et al. 2015). A large variety of oscillatory phenomena has been observed in plage regions, and they exhibit a range of periods, extending from tens of seconds up to a few minutes (De Pontieu et al. 2007; Morton et al. 2014; Morton & McLaughlin 2014; Gafeira et al. 2017; Jafarzadeh et al. 2017; Kayshap et al. 2020, also see the review by Jess et al. 2015).

In the present article, we describe the analysis of the distribution of oscillations over a range of periods in an active region (NOAA AR12651) plage observed jointly with the Atacama Large Millimeter/Submillimeter Array (ALMA; Wootten & Thompson 2009), the Interface Region Imaging Spectrograph (IRIS; De Pontieu et al. 2014), and the Atmospheric Imaging Assembly (AIA; Lemen et al. 2012) on board the Solar Dynamics Observatory (SDO). These coordinated solar observations of ALMA with IRIS and SDO provide a unique

opportunity to study the solar atmosphere at millimeter wavelengths in conjunction with the ultraviolet part of the solar spectrum. ALMA observes the continuum emission in the millimeter wavelength range and provides a direct measurement of gas temperature that is equivalent to the recorded brightness temperature.

Solar observations with ALMA have, so far, mostly been taken in Band 3 (centered at around 100 GHz ; 3 mm) and Band 6 (centered at around 239 GHz ; 1.25 mm), which are predicted to sample the mid-to-high chromosphere (Wedemeyer et al. 2016; Bastian et al. 2017; Nindos et al. 2018; Jafarzadeh et al. 2019; Loukitcheva 2019; Martínez-Sykora et al. 2020). Recent studies have also indicated that the ALMA observations may have some contributions from the transition region and lower coronal heights (Wedemeyer et al. 2020; Chintzoglou et al. 2021a,b). For more details about the solar observations with ALMA and recent results, we refer the reader to the reviews by Wedemeyer et al. (2016) and Loukitcheva (2019).

In this study we explore the presence of possible associations of ALMA observations with chromospheric and lower coronal observations from IRIS and AIA from the point of view of oscillations. The plage region studied is shown in the top panels of Fig. 1 within a larger field-of-view (FoV) of a representative Helioseismic and Magnetic Imager (HMI; Scherrer et al. 2012) line-of-sight magnetogram and an AIA 171 Å image. The first frames of the studied FoV of the different passbands are shown in the bottom panels. The article is structured as follows: in Sect. 2 we provide details of the joint observations and the applied data processing and co-alignment techniques. In Sect. 3 we explain the data-analysis technique used (Lomb-Scargle transform). We present our results in Sect. 4, a discussion in Sect. 5, and conclusions in Sect. 6.

2. Observations

This work primarily utilizes ALMA cycle 4 solar observations of a plage region in NOAA AR12651 (project 2016.1.00050.S) in Band 6 (centered at around 239 GHz ; 1.25 mm). The target, centered at $(x,y) = (-265', 265')$, was sampled between 15:59-16:34 UT on 2017 April 22 with a 2-s cadence in four blocks of approximately 8–9 min duration each, with gaps of 1.5–2 min in between for calibrations. The time sequence of the ALMA observations (brightness temperature light curve) at one pixel location is shown in the first panel of Fig. 2. The light curve shows the presence of the three episodes of data gaps.

The ALMA data set was calibrated using the Solar ALMA Pipeline (SoAP; Szydlarski et al., in prep.; also see Wedemeyer et al. 2020 for more details), which has been developed based on the Common Astronomy Software Applications (CASA) package (McMullin et al. 2007). The calibrations include the CLEAN algorithm as implemented by Rau & Cornwell (2011), self-calibration for a time window of 14 s, primary beam correction, and a combination of the interferometric data with the total power maps ("feathering" procedure). The abovementioned calibration steps finally provide the ALMA brightness temperature maps. Further details about SoAP are available in Jafarzadeh et al. (2019, 2021).

The ALMA observations were supported by co-observations of the same region by IRIS. For further details about the joint ALMA and IRIS observations, we refer the reader to da Silva Santos et al. (2020) and Chintzoglou et al. (2021a,b), in which the same coordinated ALMA and IRIS observations are analyzed. This coordinated data set is one of the first campaigns where joint observations between ALMA and IRIS were con-

ducted and good alignment between the ALMA and IRIS data sets was achieved (Henriques et al. 2022). Considering the continuous observations by AIA/SDO in a wide range of wavelengths along with the joint ALMA and IRIS observations, in this work we have been able to sample the oscillations in the plage region at multiple atmospheric heights, from the solar chromosphere to the corona.

In the present work we have used AIA observations in the 1600 Å, 304 Å, 131 Å, 171 Å, 193 Å, and 211 Å passbands and IRIS 2796 Å slit-jaw images (SJIs) with the ALMA Band-6 observations (see Fig. 1). All the images from IRIS and AIA have been aligned (spatially and temporally) with those from ALMA brightness temperature maps. For this, the IRIS and AIA images were rescaled to the sampling resolution of the ALMA maps (0.14′) prior to making spatial alignments to the same FoV. The images from the IRIS and AIA were, however, analyzed with their original spatial resolution (i.e., they were not convolved with the point spread function of ALMA). To match the higher cadence of the ALMA images, the images in the utilized IRIS and AIA time series were repeated in time when necessary.

3. Data analysis

We employed Lomb-Scargle (LS) transforms (Scargle 1982; Press & Rybicki 1989) to detect and characterize the oscillations present in the ALMA Band-6 brightness-temperature maps of the plage region. This method is particularly suitable for cases where the observation times are unevenly spaced, such as in the present ALMA observations (as mentioned in Sect. 2; also see Fig. 2). We used the standard Interactive Data Language (IDL) routine LNP_TEST to perform LS transforms with the statistical significance test of the detected periodicities against the hypothesis of the presence of random (white) noise in the input signal.

An LS transform was performed at each pixel location in the ALMA FoV to extract the information about the distribution of power in different periodicities over the observed plage region. Figure 2 shows a representative example of the results from the LS analysis corresponding to the pixel location at the center of the FoV. The top panel in Fig. 2 shows the variation in the ALMA brightness temperature (light curve) with time. The instances of data gaps along the light curve are shown in the top and middle panels.

The middle panel shows the light curve after removal of the linear background trend (dashed line in the first panel) and apodization, which is further used to obtain the periodogram shown in the bottom panel. The trend subtraction helps to remove the periodicities that can arise due to non-stationary data. The data were then apodized using a Tukey window to remove the edge effects. To increase the frequency resolution, the signal was padded with zeros (at one end) prior to the LS transform. The padding was performed such that it increased the length of the signal by a factor of 5. The bottom panel displays the periodogram showing power spectrum (solid line) with the 95% confidence level (dotted line). We further used the periodograms obtained at every location in the FoV to study the spatial distribution of ALMA oscillations and its association with those from IRIS and AIA observations.

The power spectrum obtained in the particular example in Fig. 2 has a prime dominant power peak at a period of 3.3 min. The second strong (dominant) power peak, at around 13.7 min, is only slightly lower than that at 3.3 min. The power spectrum also constitutes multiple weaker, yet significant, peaks. It is thus worth noting that the dominant period estimation may be biased when more than one strong peak occurs in a power spectrum.
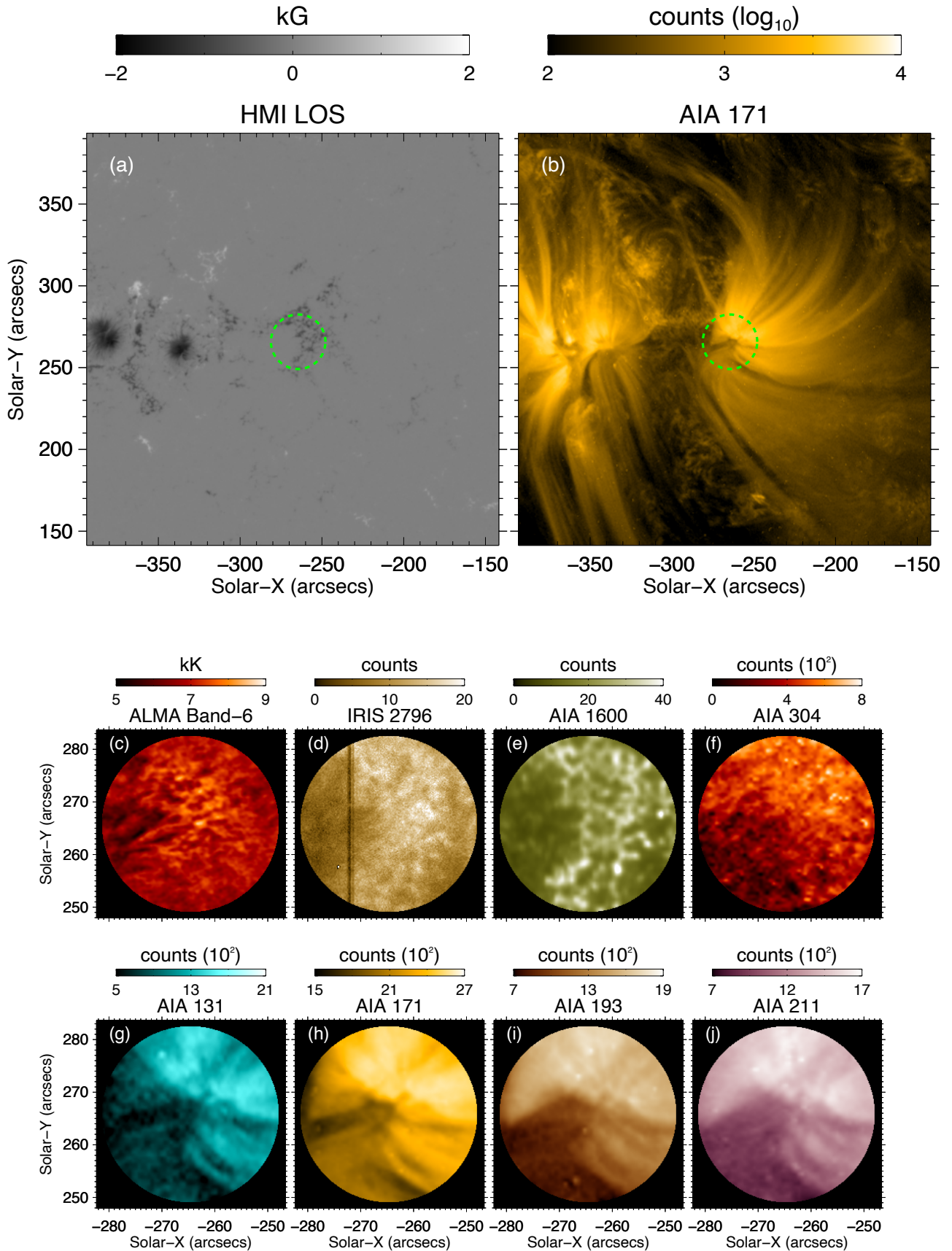
Fig. 1. Context images showing the HMI line-of-sight (LOS) magnetogram in *panel a* and the AIA 171 Å image in *panel b* at the start time of the ALMA observations. The FoV studied here is marked by the green circle in *panels a and b*. Panels *c–j*: show the representative images of the studied FoV (from ALMA Band 6, IRIS SJI 2796 Å, and different AIA channels, as indicated on top of the panels) at the start time of the observations.
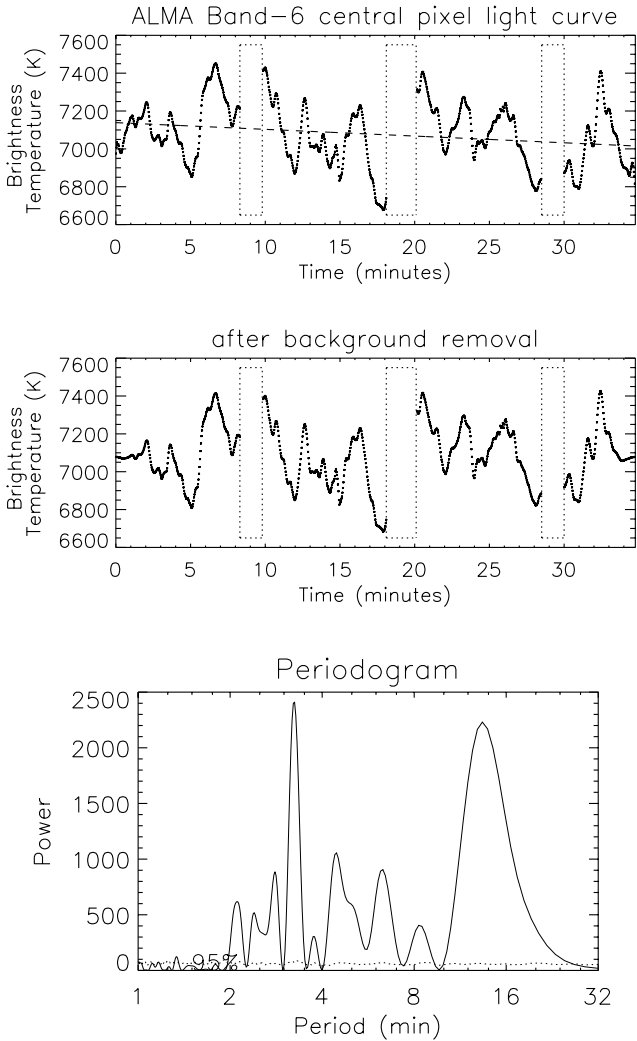
Fig. 2. Lomb-Scargle analysis for the ALMA Band-6 brightness temperature variation with time at the pixel location at the center of the FoV. *Top panel*: light curve of the ALMA brightness temperature (black symbols) with the background trend (dashed line) and data gaps marked within dotted boxes. *Middle panel*: apodized and de-trended light curve. *Bottom panel*: periodogram showing the power spectrum (solid line) with the 95% confidence level (dotted line).

Thus, they should be interpreted with great caution (i.e., a dominant period does not necessarily represent the period at the strongest power peak, but rather the period at one of the strong power peaks). This should not, however, affect the overall statistical associations, which we study in the following sections. This is elaborated further in Sect. 4.1.1.

4. Results

4.1. Distribution of dominant period

4.1.1. Global behavior

The dominant period (period at peak power in the periodogram) was determined for every pixel location in all the passbands. The global behavior of the preferential dominant period in the different passbands was studied by means of histograms and average power spectra, as shown in Fig. 3. The different panels in Fig. 3 show the histograms of the dominant periods for the different passbands. Overplotted are the respective average power spec-

tra (averaged over all power spectra determined at all individual pixels). As mentioned in Sect. 3, the dominant period estimation could be biased at pixels where more than one dominant peak is observed in their power spectra. However, from the statistical point of view, this should likely not affect the overall global trends. This is justified in Fig. 3, where the variations (appearances of peaks) in the histograms and the corresponding average spectra are in good agreement, demonstrating that the estimated dominant periods represent the average state of the oscillations well. It should be noted that all of the average power spectra show the expected rising trend with increasing period (also see Fig. 4). Though we have obtained the dominant period values up to ~35 min, we restricted the analysis to up to 20 min. This is due to the fact that the longer dominant periods detected can be related to the long-term evolution of the various features in the atmosphere and not to oscillations.

The ALMA histogram in panel (a) of Fig. 3 shows that most of the locations in the ALMA FoV have a dominant period of oscillation in the 12–14 min period range. In contrast, the histograms of the IRIS 2796 Å passband in panel (b) and the AIA 1600 Å passband in panel (c) (sampling heights approximately corresponding to the middle chromosphere and low chromosphere, respectively) show the prominent dominant oscillations to be in the 4–6 min period range. This contrast is also evident from Fig. 4, where the power spectra for all the passbands are shown together for a better comparison. It is important to note here that we were unable to perform any comparisons of ALMA oscillations with those present in the upper chromospheric layers due to the following limitation of the observations. The upper chromosphere and transition region can typically be observed by IRIS SJIs in the 1330 Å and 1400 Å passbands. Though the data set used here contains the slit-jaw observations in these passbands, the signal in these passbands is too poor in this observation set to be considered for any time-frequency transform, including LS. These slit-jaw observations are underexposed, with an average count of two and four in the 1300 Å and 1400 Å passband, respectively.

The oscillations with ~3 min periods in the chromosphere are well understood and are explained as the basic cutoff frequency resonance of the chromosphere (Deubner & Fleck 1990; Fleck & Schmitz 1991; Carlsson & Stein 1994; Rutten 1995). As mentioned in Sect. 1 (and citations therein), various numerical models and simulations have predicted ALMA to probe plasma conditions in the mid-to-high chromosphere. The very different global behavior of ALMA oscillations observed here indicates the need for more detailed investigations to determine the formation height of the radiation observed by ALMA. The absence of dominant 3–5 min oscillations in the ALMA observations has been discussed in Jafarzadeh et al. (2021) (a more detailed study will be presented in Jafarzadeh et al., in prep.).

The transition region passband of AIA 304 Å can have contributions from the higher chromosphere up to the lower corona. The histogram for AIA 304 Å in panel (d) of Fig. 3 shows two peaks; while the one at 6–8 min is the more prominent, the other at 12–14 min is comparable. The peak around 12–14 min is also present in the histograms of all the coronal passbands of AIA in panels (e) to (h). As the ALMA histogram in panel (a) also shows a prominent dominant period in the 12–14 min range, it can be conjectured that the global behavior of ALMA oscillations may have an association with the transition region and lower coronal oscillations, rather than with the chromosphere. The presence of possible spatial correlations, if any, are further investigated in more detail in the following sections.
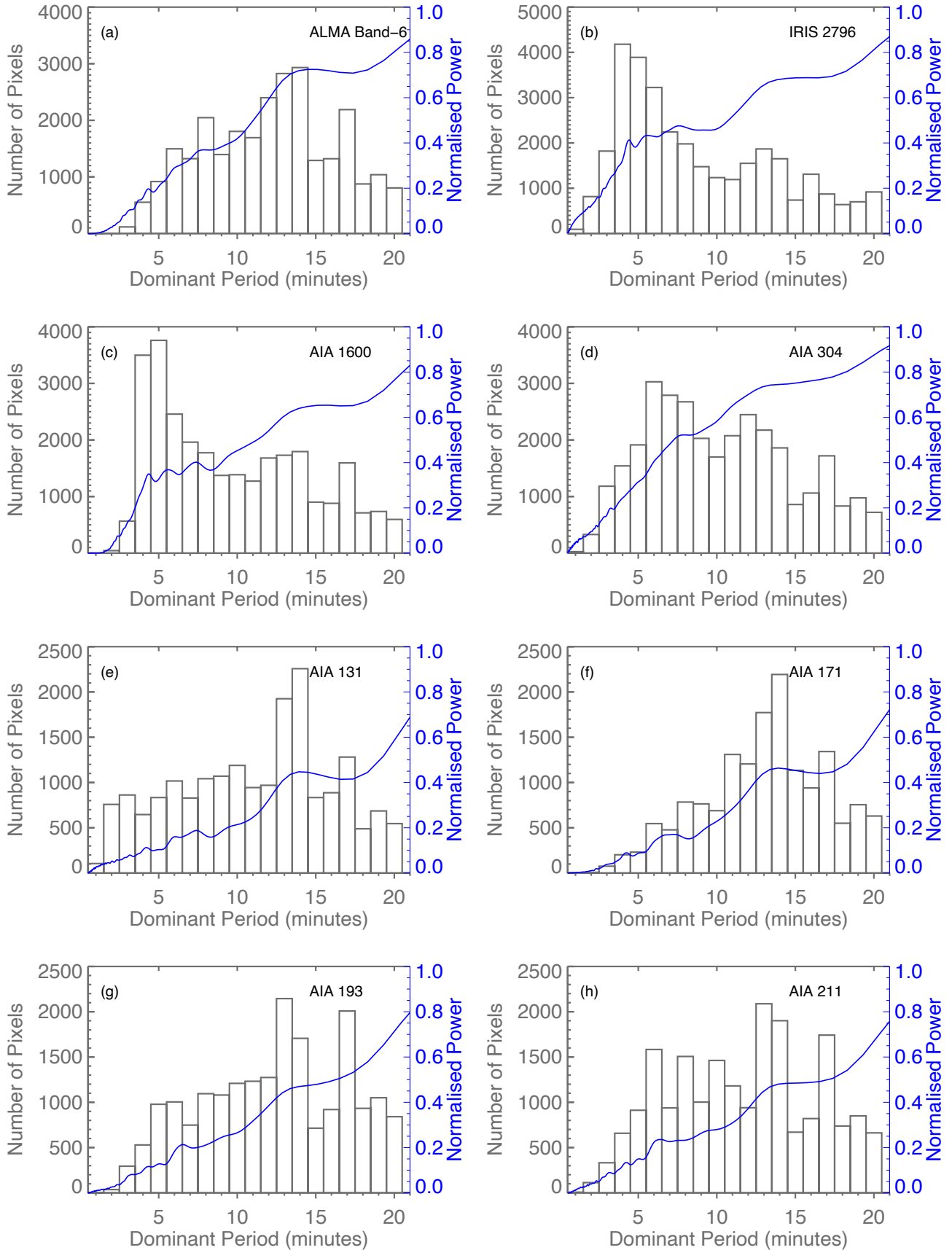
Fig. 3. Histograms of dominant periods (grey) detected over the FoV in the different passbands. Overplotted in blue are the average power spectra for the respective passband.
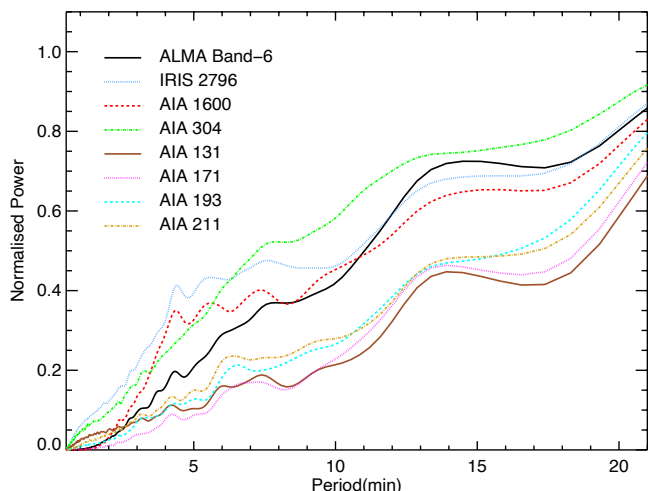
Fig. 4. Average power spectra of the eight passbands shown in Fig. 3.

4.1.2. Spatial correlation

We further studied the association of dominant periods in ALMA oscillations with those of IRIS and AIA by means of dominant period maps. A dominant period map shows the spatial distribution of the dominant period over the FoV. The dominant periods (period at peak power in the periodogram) are determined for every pixel location for all passbands and are shown in Fig. 5 for the entire FoV of the different passbands. By means of scatter plots we studied the correlation of the ALMA dominant period map with the other passbands. Figure 6 shows the different scatter plots with the value of cross-correlation coefficients between the respective full FoV dominant period maps. We do not observe any statistical trends or patterns in the scatter plots.

We further partitioned the FoV into two sub-regions (shown in Fig. 5), the bright plage region and the peripheral region, based on the intensity threshold from AIA 1600 Å observations (see Appendix A for details). The association among the dominant period was then further studied, in a similar manner as described above, separately in the bright plage region and the peripheral region. The dominant period histograms and the average LS power spectra obtained separately for the bright plage and the peripheral region do not show different trends in comparison to each other for the respective passbands. Those trends are also similar to the ones obtained for the full FOV that were shown in Figs. 3 and 4. Figures 7 and 8 show the scatter plots between the ALMA dominant period map with the other passbands for the bright plage region and the peripheral region, respectively. The scatter plots in Figs. 6–8 show the absence of any spatial correlation of the dominant oscillations in ALMA observations with those in other passbands. The very low values of the cross-correlation coefficients (less than 6%) for all cases indicate that the distribution of the dominant periods of the ALMA oscillations does not have a direct association with those of IRIS and AIA (in these particular observations).

The analysis above, involving the dominant period maps, may be hiding some correlations, particularly for the short-period oscillations. As mentioned earlier, the longer dominant periods (more than 20 min) in the dominant period maps could be arising due to the long-term evolution of the various features, which can be unrelated to one another at different atmospheric heights. This can result in low cross-correlation values. To avoid the effects of the long-term evolution, we further studied the association of ALMA oscillation power with that of other pass-

bands in separate period bins by means of power maps. The analysis in Sect. 4.2 also enabled us to study the correlation of the oscillations in the respective period intervals, in contrast to this section, where we only studied the dominant oscillation periods.

4.2. Distribution of oscillation power

To further explore the interrelation of ALMA oscillations with the other chromospheric transition region and lower coronal observations, we studied the association of the distribution of ALMA oscillation power with that of the IRIS and AIA oscillations. The power maps show the value of the power averaged over the desired period interval in the periodogram at each pixel location over the FoV. We obtained power maps in six period bins (1–2 min, 2–4 min, 4–6 min, 6–10 min, 10–15 min, and 15–20 min) for all data sets. Figure 9 shows the power maps for ALMA, IRIS 2796 Å, and different passbands of AIA in the six period bins. Since we are interested in the comparison of power distributions within respective period bins of different data sets, every power map is normalized to its maximum value.

The power maps of ALMA do not show any close association with the power maps of IRIS 2796 Å and the different AIA passbands. This is depicted in Fig. 10, where the scatter plots between the entire FoV power maps of ALMA and other passbands, in the six period bins, are shown. The value of the cross-correlation coefficients between the respective power maps are also given in the scatter plots. The scatter plots show the absence of any kind of statistical trend or relation of ALMA oscillation power with that of IRIS and AIA. The corresponding scatter plots, obtained separately for the bright plage region and the peripheral region, also show very low cross-correlation values, less than 12% for most of the cases. All the above analyses strongly indicate a lack of any association between oscillations observed with ALMA and those observed with IRIS and AIA, the possible reasons for which are discussed in the next section.

5. Discussion

We speculate that the low correlations are possibly due to the large variations in formation height of the millimeter continuum about 1.25 mm observed by ALMA Band 6. Such large formation-height variations may also be present in the other wide-band images analyzed here. As mentioned in Sect. 1 (and citations therein), the numerical models have predicted ALMA to sample the mid-to-high chromosphere, although the exact heights of the formation of the ALMA signal remain to be uncovered. Loukitcheva et al. (2015) employed Bifrost numerical simulations (Gudiksen et al. 2011) to discuss the effects of the broad contribution functions of different ALMA bands in general. They discussed that the brightness temperatures deduced from ALMA observations represent the integrated physical state of the atmosphere over an extended height range (~500 km). They have shown that, depending on the underlying magnetic structure, the contribution functions of the ALMA bands can have distinct multiple peaks representing different, well-separated height ranges. Their analysis also shows that in the regions with a strong magnetic field, the millimeter observations tend to map comparatively higher atmospheric layers than the surrounding weaker magnetic field locations. Similar results have also recently been shown by Eklund et al. (2021), who also investigated the different ALMA bands in the Bifrost simulations and provided the distributions of their formation heights in various solar regions with different levels of chromospheric
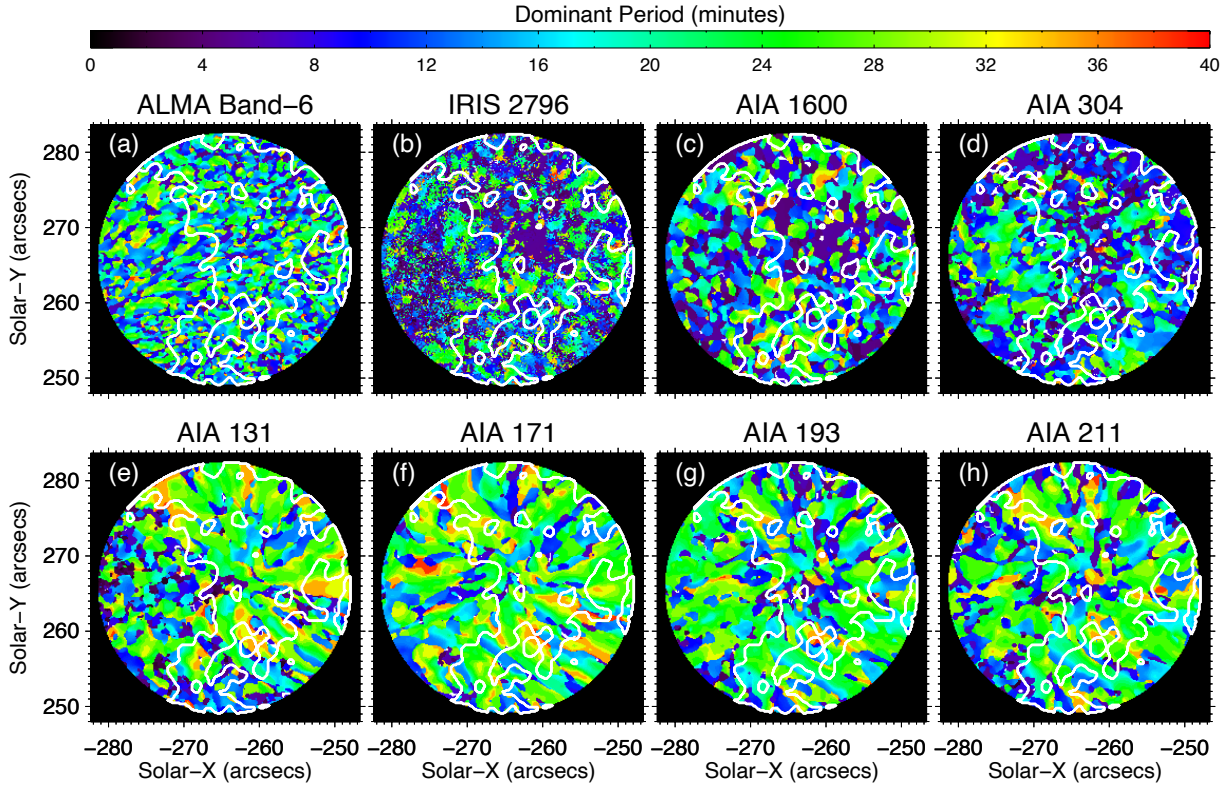
Fig. 5. Dominant period maps of the different passbands studied. The white contours enclose the bright plage region, and the surrounding area (outside the contours) is termed as the peripheral region.
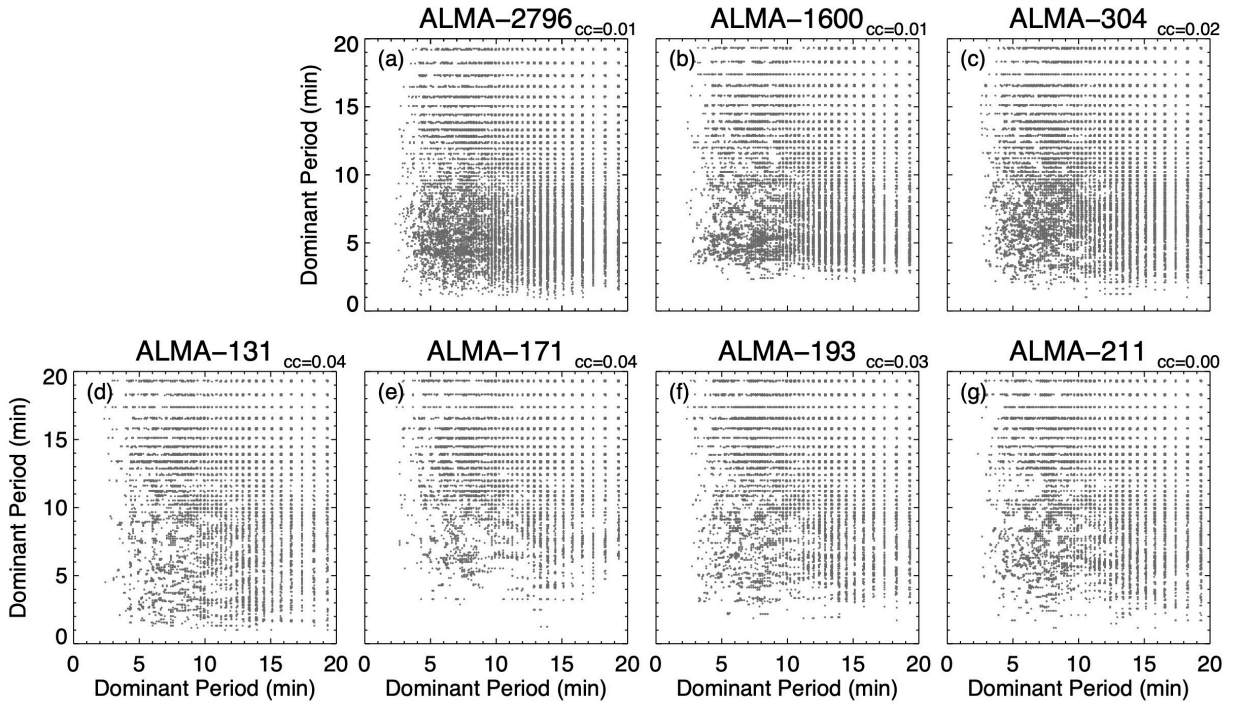

Fig. 6. Scatter plots, for the full FoV, of the ALMA Band-6 dominant period map shown along with that from IRIS 2796 Å in *panel a* and different AIA channels in *panels b–g*. The value of the cross-correlation coefficient ("cc") is shown to the top right of each panel.

magnetic flux. They found a range of about 500–2000 km for the synthetic ALMA Band-6 images, with a larger peak occurring toward the higher end in the more magnetically active regions. Such large variations in formation height can create strong temporal modulations that could destroy the oscillatory signals at particular periods (e.g., at around 3 min).

Rutten (2017) and Jafarzadeh et al. (2021) discussed the role that magnetic-field strength and topology may play in the propagation of magnetoacoustic waves in the chromosphere. In particular, Jafarzadeh et al. (2021) performed a statistical study of ALMA oscillations using ten different data sets (from both Band 3 and Band 6) and found that the behavior of ALMA oscillations
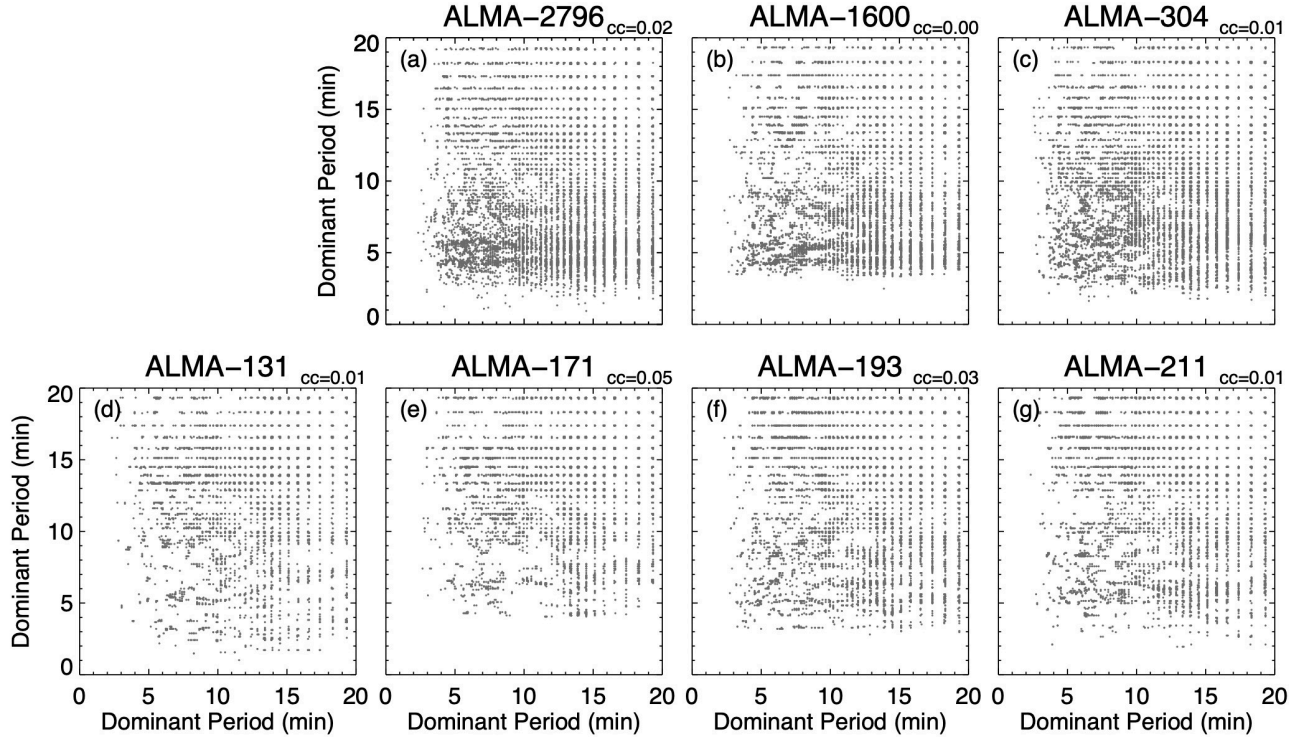
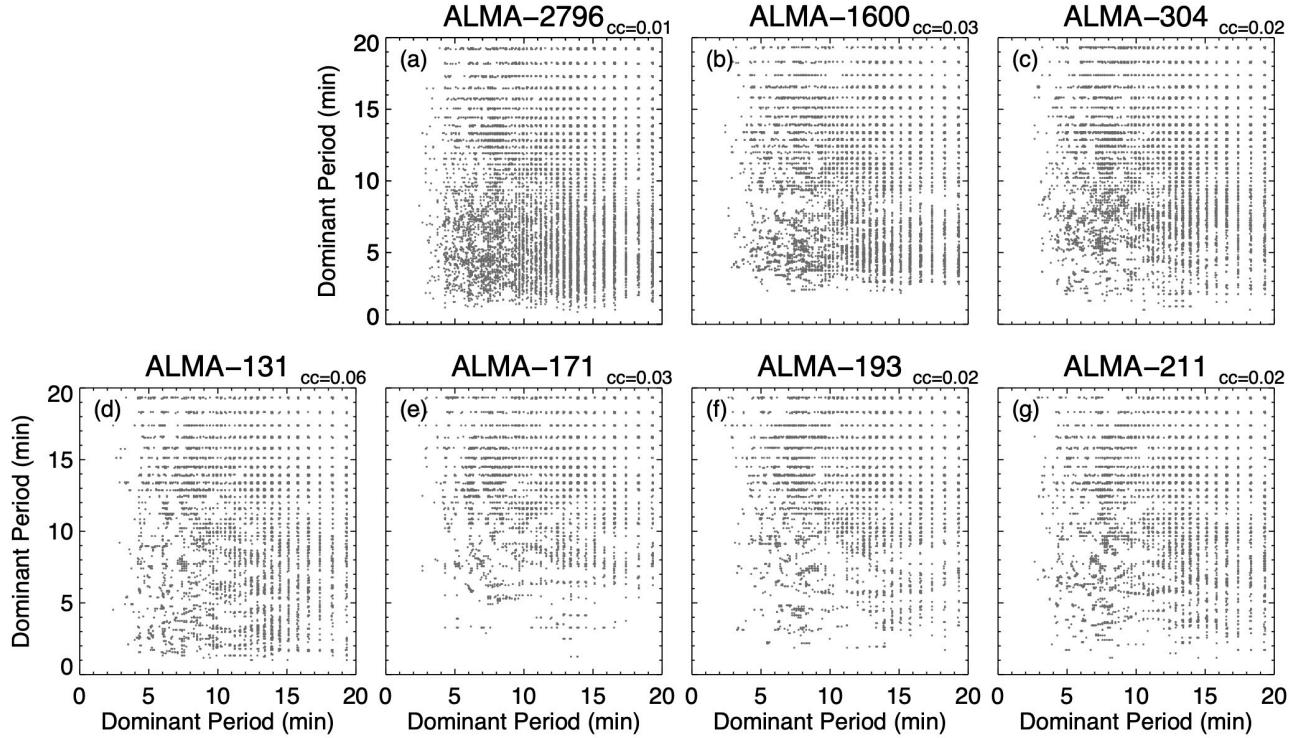**Fig. 7.** Same as Fig. 6 but only for the bright plage region of the FoV.

Fig. 8. Same as Fig. 6 but only for the peripheral region of the FoV.

is only similar to that of AIA 1600 Å in the most magnetically quiescent data sets, with the presence of 3–5 min oscillations, whereas the data sets influenced by higher magnetic flux (i.e., the presence of active and/or plage regions inside and/or in the immediate vicinity of the observed FoVs) showed a lack of 3–5 min oscillations and had average power peaks at longer periods. In the present study, while we also find no clear 3–5 min

oscillations in the ALMA Band-6 observations, such oscillations were observed in both the AIA 1600 Å and IRIS SJI 2796 Å data sets. While the former samples heights corresponding to the low chromosphere, the latter is supposedly formed around the middle chromosphere. Thus, if the magnetic canopy acted as an obscuring effect, or if the large magnetic strength suppressed the power at shorter periods as discussed by Jafarzadeh et al. (2021) for the
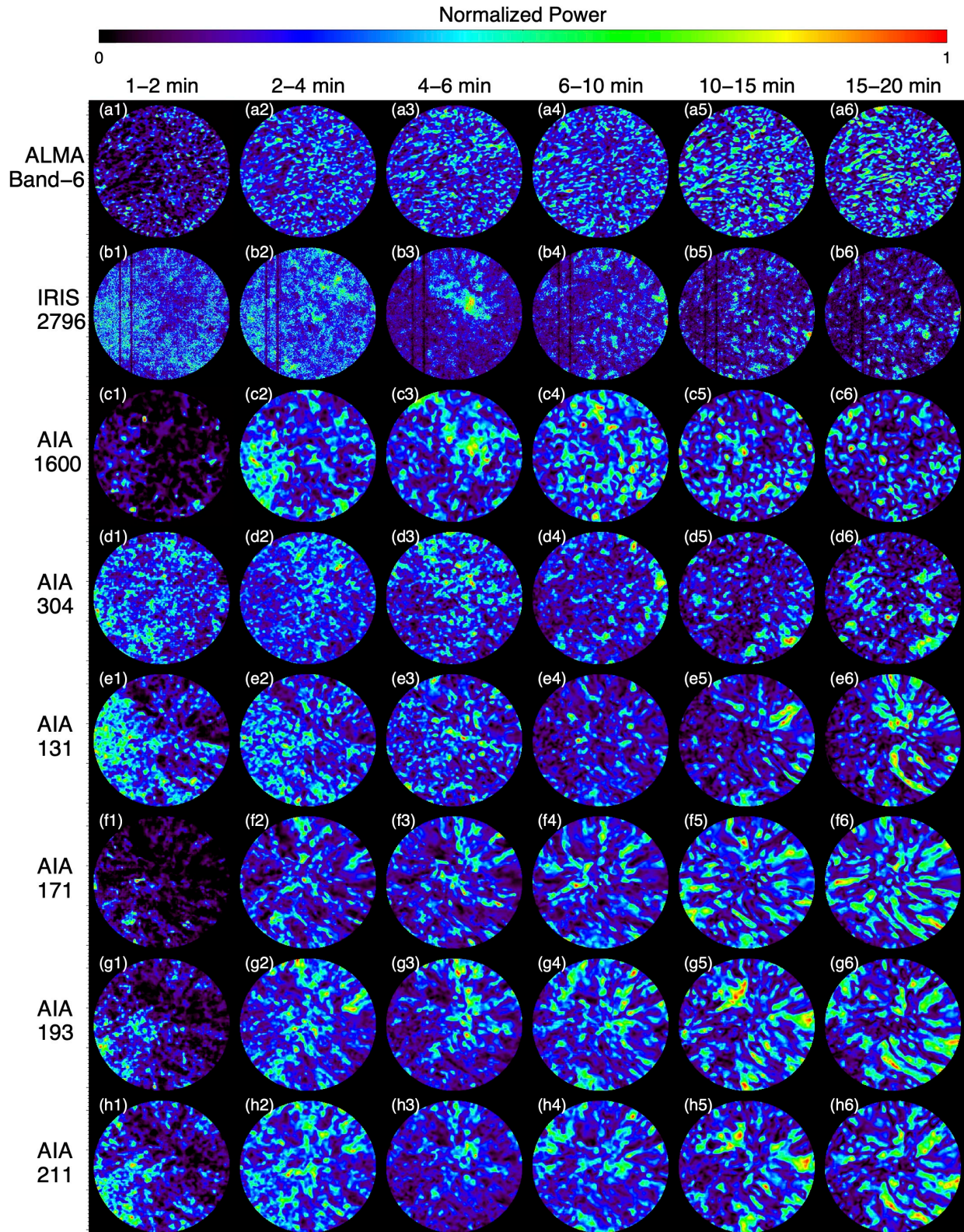
Fig. 9. Power maps of different passbands in the six period intervals.

ALMA observations, they should also similarly influence other chromospheric observations, such as those with IRIS SJI 2796 Å, if both were formed at similar heights. However, as noted above, the exact heights of formation of the ALMA observations are still unknown. In addition, the IRIS SJIs were obtained using relatively broadband filters and may include contributions from a large range of heights. How the heights of formation of the ALMA Band 6 and IRIS SJI 2796 Å passbands are compared could serve as the key to understanding the discrepancy. Also, further studies using narrowband observations sampling various heights throughout the solar chromosphere can clarify the speculations mentioned above.
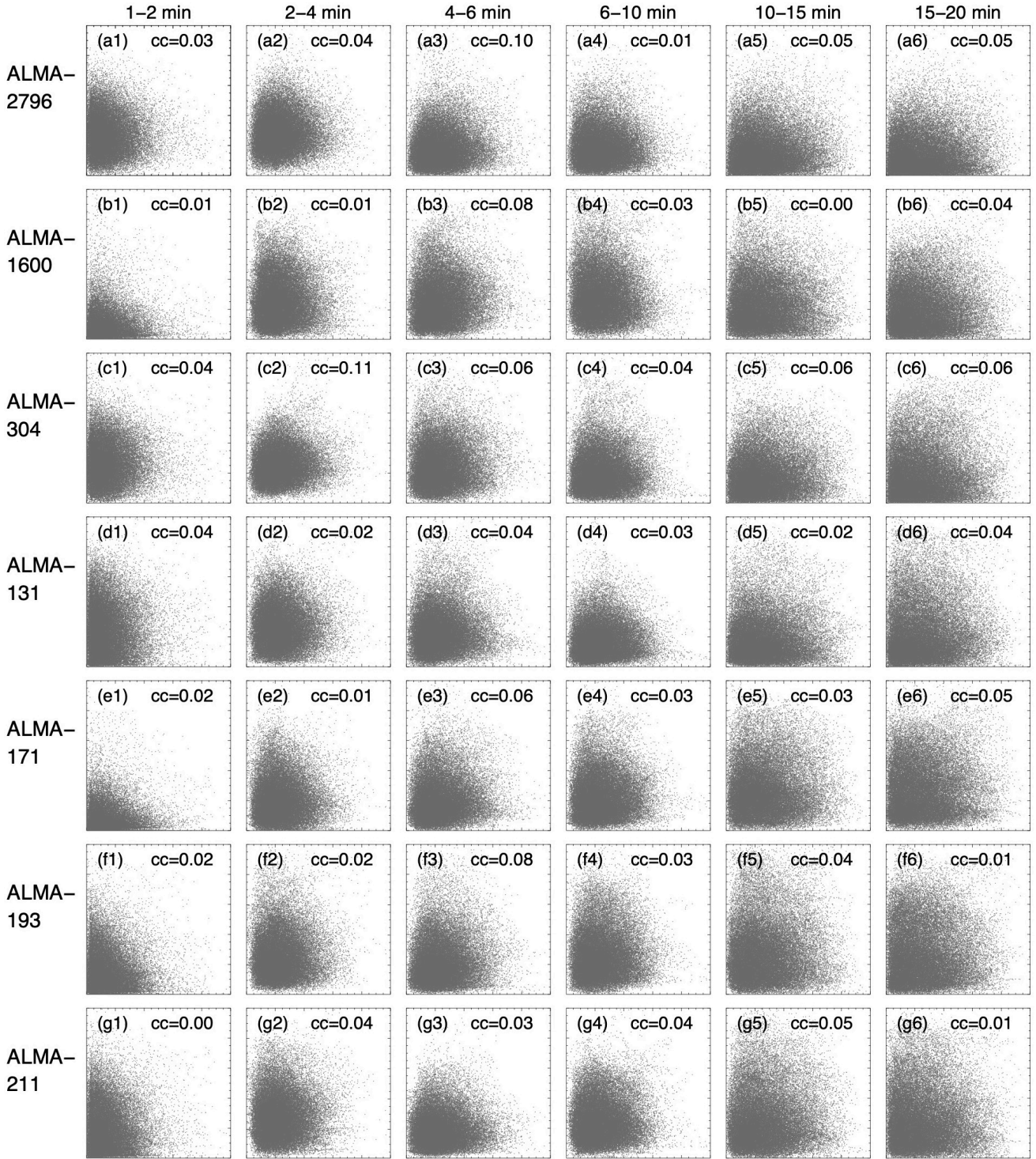
Fig. 10. Scatter plots, for the full FoV, of ALMA Band-6 power maps in the six period intervals shown along with those from IRIS 2796 Å in *panels a1–a4* and different AIA channels in *panels b1–g4*. The value of the cross-correlation coefficient ("cc") is shown at the top right of each panel.

Recent studies have also indicated that ALMA observations may have some contributions from the transition region and corona (Wedemeyer et al. 2020; Chintzoglou et al. 2021a,b). It is thus likely that the ALMA observations have simultaneous oscillatory contributions from a range of geometrical heights, from the chromosphere to the corona. Furthermore, it is important to note that ALMA observations map the brightness temperature fluctuations, which are estimated from the continuum intensity

under the Rayleigh-Jeans limit. This is in contrast to the intensity fluctuations observed in broadband filter images by IRIS and AIA, which depend on the collective behavior of the plasma temperature and density. The temperature and density oscillations may have complex phase relations depending on the frequency and wave mode and the thermodynamical conditions in the different atmospheric layers, with adiabatic conditions dominant in the chromosphere and isothermal conditions in the corona

(Severino et al. 2013; Van Doorsselaere et al. 2011). With the possibility of ALMA sampling these very different thermo-dynamical environments simultaneously, with non-equilibrium effects prevalent in the chromosphere and transition region, the coupling between ALMA temperature oscillations and IRIS/AIA intensity oscillations may become complex, which could explain the observed lack of association between ALMA temperature and IRIS/AIA intensity oscillations.

6. Conclusions

This article showcases a statistical comparison of the power distribution of oscillations in a plage region that spans the solar atmosphere from the chromosphere to the lower corona, utilizing coordinated observations from ALMA, IRIS, and SDO. We performed LS transforms to statistically characterize the oscillations in ALMA Band-6 (1.25 mm), IRIS 2796 Å SJI, and AIA 1600 Å, 304 Å, 131 Å, 171 Å, 193 Å, and 211 Å observations. The distribution of the dominant period reveals the presence of oscillations over a wide range of periods (up to 35 min), with 12–14 min prominent in the ALMA and AIA coronal passbands (Figs. 3–5). On the other hand, the chromospheric and transition region passbands of IRIS and AIA show a prominence of shorter periods of about 4–7 min. It is worth noting that while here we are discussing the global dominant behavior of oscillations, a large range of oscillation periods can be dominant in some of the individual features, as shown in the dominant period maps in Fig. 5. The detection of high-frequency oscillations (<2 min) have also been reported by Guevara Gómez et al. (2021) and Eklund et al. (2020) in some specific features in ALMA Band-3 observations.

The ALMA oscillations in the plage region studied here are observed not to be associated with those observed by IRIS SJI and AIA. As shown in the scatter plots in Figs. 6–8, and 10, the ALMA dominant period map and power maps over the range of periods (up to 20 min) do not show any spatial correlation with the respective ones from the other passbands, with all the cross-correlation coefficients less than 0.12. A better understanding of the range of the formation height of the millimeter continuum observed by ALMA will help to explain the specific reasons for such non-associated behavior of ALMA oscillations with the IRIS and AIA oscillations. Additionally, the complex inter-relation between the nature of ALMA temperature oscillations with the IRIS/AIA intensity oscillations need to be explored in detail. Further statistical investigations using multiple coordinated observations spanning a variety of solar features in quiet Sun, coronal hole, and active regions, complemented with numerical models, should help to better understand the nature of the oscillations observed with ALMA, and thus its association with other observations.

References

Arregui, I. 2015, Philos. Trans. R. Soc. London Ser. A, 373, 20140261
Bastian, T. S., Chintzoglou, G., De Pontieu, B., et al. 2017, ApJ, 845, L19
Brynildsen, N., Maltby, P., Brekke, P., Redvik, T., & Kjeldseth-Moe, O. 2003, Adv. Space Res., 32, 1097
Carlsson, M., & Stein, R. F. 1994, in Chromospheric Dynamics, ed. M. Carlsson, 47
Carlsson, M., Leenaarts, J., & De Pontieu, B. 2015, ApJ, 809, L30
Carlsson, M., De Pontieu, B., & Hansteen, V. H. 2019, ARA&A, 57, 189
Chintzoglou, G., De Pontieu, B., Martínez-Sykora, J., et al. 2021a, ApJ, 906, 82
Chintzoglou, G., De Pontieu, B., Martínez-Sykora, J., et al. 2021b, ApJ, 906, 83
da Silva Santos, J. M., de la Cruz Rodríguez, J., Leenaarts, J., et al. 2020, A&A, 634, A56
De Pontieu, B., Hansteen, V. H., Rouppe van der Voort, L., van Noort, M., & Carlsson, M. 2007, ApJ, 655, 624
De Pontieu, B., Title, A. M., Lemen, J. R., et al. 2014, Sol. Phys., 289, 2733
Deubner, F. L., & Fleck, B. 1990, A&A, 228, 506
Eklund, H., Wedemeyer, S., Szydlarski, M., Jafarzadeh, S., & Guevara Gómez, J. C. 2020, A&A, 644, A152
Eklund, H., Wedemeyer, S., Szydlarski, M., & Jafarzadeh, S. 2021, A&A, 656, A68
Fleck, B., & Schmitz, F. 1991, A&A, 250, 235
Gafeira, R., Jafarzadeh, S., Solanki, S. K., et al. 2017, ApJS, 229, 7
Gilchrist-Millar, C. A., Jess, D. B., Grant, S. D. T., et al. 2021, Philos. Trans. R. Soc. London Ser. A, 379, 20200172
Gudiksen, B. V., Carlsson, M., Hansteen, V. H., et al. 2011, A&A, 531, A154
Guevara Gómez, J. C., Jafarzadeh, S., Wedemeyer, S., et al. 2021, Philos. Trans. R. Soc. London Ser. A, 379, 20200184
Henriques, V. M. J., Jafarzadeh, S., Guevara Gómez, J. C., et al. 2022, A&A, 659, A31
Jafarzadeh, S., Solanki, S. K., Feller, A., et al. 2013, A&A, 549, A116
Jafarzadeh, S., Solanki, S. K., Gafeira, R., et al. 2017, ApJS, 229, 9
Jafarzadeh, S., Wedemeyer, S., Szydlarski, M., et al. 2019, A&A, 622, A150
Jafarzadeh, S., Wedemeyer, S., Fleck, B., et al. 2021, Philos. Trans. R. Soc. London Ser. A, 379, 20200174
Jess, D. B., Morton, R. J., Verth, G., et al. 2015, Space Sci. Rev., 190, 103
Kayshap, P., Srivastava, A. K., Tiwari, S. K., Jelínek, P., & Mathioudakis, M. 2020, A&A, 634, A63
Lemen, J. R., Title, A. M., Akin, D. J., et al. 2012, Sol. Phys., 275, 17
Loukitcheva, M. 2019, Adv. Space Res., 63, 1396
Loukitcheva, M., Solanki, S. K., Carlsson, M., & White, S. M. 2015, A&A, 575, A15
Martínez-Sykora, J., De Pontieu, B., de la Cruz Rodriguez, J., & Chintzoglou, G. 2020, ApJ, 891, L8
McMullin, J. P., Waters, B., Schiebel, D., Young, W., & Golap, K. 2007, in Astronomical Data Analysis Software and Systems XVI, eds. R. A. Shaw, F. Hill, & D. J. Bell, ASP Conf. Ser., 376, 127
Morton, R. J., & McLaughlin, J. A. 2014, ApJ, 789, 105
Morton, R. J., Verth, G., Jess, D. B., et al. 2012, Nat. Comm., 3, 1315
Morton, R. J., Verth, G., Fedun, V., Shelyag, S., & Erdélyi, R. 2013, ApJ, 768, 17
Morton, R. J., Verth, G., Hillier, A., & Erdélyi, R. 2014, ApJ, 784, 29
Nakariakov, V. M., & Verwichte, E. 2005, Liv. Rev. Sol. Phys., 2, 3
Narain, U., & Ulmschneider, P. 1990, Space Sci. Rev., 54, 377
Narain, U., & Ulmschneider, P. 1996, Space Sci. Rev., 75, 453
Nindos, A., Alissandrakis, C. E., Bastian, T. S., et al. 2018, A&A, 619, L6
Press, W. H., & Rybicki, G. B. 1989, ApJ, 338, 277
Rau, U., & Cornwell, T. J. 2011, A&A, 532, A71
Rutten, R. J. 1995, in Helioseismology, eds. J. T. Hoeksema, V. Domingo, B. Fleck, & B. Battrick, ESA Spec. Publ., 376, 151
Rutten, R. J. 2017, A&A, 598, A89
Scargle, J. D. 1982, ApJ, 263, 835
Scherrer, P. H., Schou, J., Bush, R. I., et al. 2012, Sol. Phys., 275, 207
Severino, G., Straus, T., Oliviero, M., Steffen, M., & Fleck, B. 2013, Sol. Phys., 284, 297
Stangalini, M., Giannattasio, F., Erdélyi, R., et al. 2017, ApJ, 840, 19
Taroyan, Y., & Erdélyi, R. 2009, Space sci. Rev., 149, 229
Van Doorsselaere, T., Wardle, N., Del Zanna, G., et al. 2011, ApJ, 727, L32
Wedemeyer, S., Bastian, T., Brajša, R., et al. 2016, Space Sci. Rev., 200, 1
Wedemeyer, S., Szydlarski, M., Jafarzadeh, S., et al. 2020, A&A, 635, A71
Wedemeyer-Böhm, S., Lagg, A., & Nordlund, Å. 2009, Space Sci. Rev., 144, 317
Wootten, A., & Thompson, A. R. 2009, IEEE Proc., 97, 1463

Appendix A: Bright plage and peripheral region

As mentioned in Sect. 4.1.2 and shown in Fig. 5, we partitioned the FoV into two subregions, the bright plage region and the peripheral region, based on the intensity threshold from AIA 1600 Å observations. From the time-averaged AIA 1600 Å intensity image, we selected the locations with higher than average counts (average over the FoV) as the bright plage region. The remaining region of the FoV was assigned as the peripheral region. Figure A.1 shows the time-averaged AIA 1600 Å image, with the bright plage region surrounded by the peripheral region. One representative image from each of the passbands studied is shown in Fig. A.2 (similar to Fig. 1), with the bright plage region separated from the peripheral region.
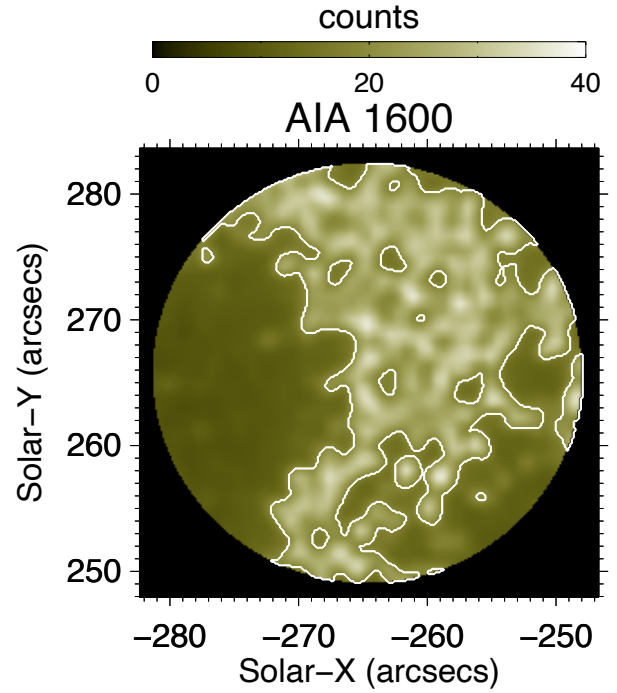

Fig. A.1. Time-averaged AIA 1600 Å intensity image of the studied FoV. Overplotted are the white contours that enclose the bright plage region. The surrounding area (outside the contours) is the peripheral region.
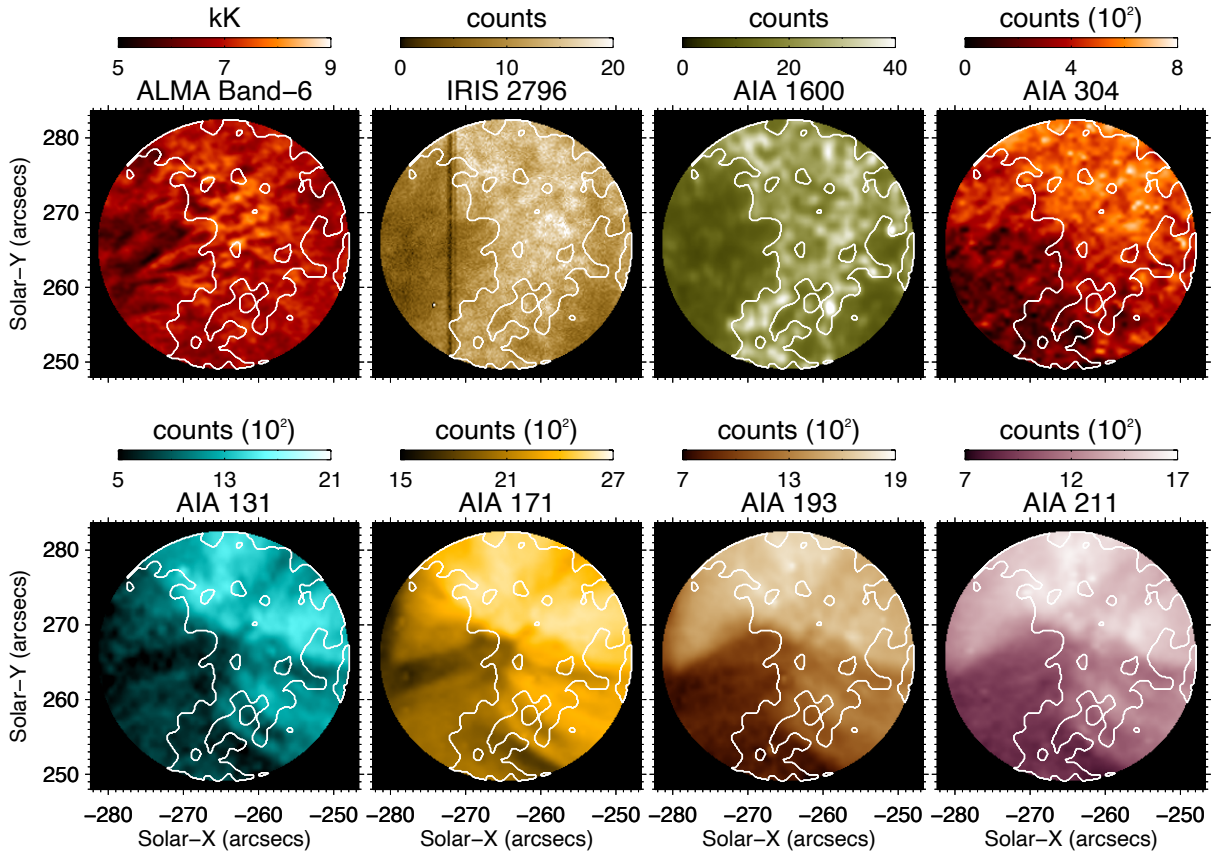

Fig. A.2. Representative images of the studied FoV (from ALMA Band 6, IRIS SJI 2796 Å, and different AIA channels, as indicated on top of the panels) at the start time of the observations. Overplotted are white contours that separate the bright plage region from the peripheral region.